Cyclostationary Noise Analysis of Large RF Circuits with Multitone Excitations

Jaijeet Roychowdhury, David Long, and Peter Feldmann, *Senior Member, IEEE*

Abstract—This paper introduces a new, efficient technique for analyzing noise in large RF circuits subjected to true multitone excitations. Noise statistics in such circuits are time-varying, hence cyclostationary stochastic processes, characterized by *harmonic power spectral densities* (HPSD's), are used to describe noise. HPSD's are used to devise a harmonic-balance-based noise algorithm with the property that required computational resources grow almost linearly with circuit size and nonlinearity. Device noises with arbitrary spectra (including thermal, shot, and flicker noises) are handled, and input and output correlations, as well as individual device contributions, can be calculated.

HPSD-based analysis is also used to establish the nonintuitive result that bandpass filtering of cyclostationary noise can result in stationary noise.

Results from the new method are validated against Monte Carlo simulations. A large RF integrated circuit (>300 nodes) driven by a local oscillator (LO) tone and a strong RF signal is analyzed in less than two hours. The analysis predicts correctly that the presence of the RF tone leads to noise folding, affecting the circuit's noise performance significantly.

Index Terms— Cyclostationary noise, harmonic balance, harmonic power spectral density, HPSD, mixer noise, nonlinear noise analysis, RF noise.

I. INTRODUCTION

PREDICTING noise in RF circuits is a more complex task than in linear circuitry, because the former typically undergo large-signal (quasi-)periodic variations in their operation, unlike the latter. Therefore the statistics of the RF circuit's noise also vary (quasi-)periodically in time, leading to important effects such as up- and down-conversion of noise spectra. Such effects cannot be predicted by traditional SPICE-like noise simulations, which are based on linear-time-invariant (LTI) analysis of stationary noise. In order to address such effects, the time-varying nature of noise, as well as the variations of the circuit due to its large signal swings, must be considered. In this paper, a new RF noise formulation and algorithm is presented which uses cyclostationary stochastic process and linear-time-varying concepts to capture time variation.

Most previous algorithms [1]–[3] that model time-varying noise are limited to designs containing relatively few nonlinear elements, characteristic of microwave circuits. These methods are impractical for integrated RF circuits where nonlinear devices are numerous. Recently, an algorithm [4] was proposed that can analyze large circuits efficiently, but it is limited to single-tone excitations only. The technique presented in

this paper can analyze noise efficiently in large circuits with multitone large-signal inputs.

Being periodic or quasi-periodic, the statistics of cyclostationary processes can be expressed in Fourier series. The present technique is formulated in terms of the coefficients of the Fourier series, termed *cyclostationary components*. The cyclostationary components, which the new algorithm computes efficiently, are useful in system-level analysis as equivalent noise models of RF circuit blocks. They also provide an intuitive yet mathematically rigorous visualization of RF noise propagation, which can contribute to design insight.

The algorithm, an extension of the approach of Ström and Signell [5], is based on a novel block-matrix relation between the cyclostationary components of noise within a circuit. The algorithm can be used to compute the total noise at a specific output, correlations between noise at different outputs, and also individual contributions from each noise generator to a specific output. Moreover, bias-dependent white and colored noise sources (e.g., thermal, shot, and flicker noises) are treated naturally, even when they are correlated. All computations are performed efficiently, i.e., the algorithm can handle large circuits with many nonlinearities with reasonable time and memory requirements. Efficiency is maintained under multitone large-signal excitations. A two-tone+noise analysis of an RF mixer circuit with more than 300 nodes is presented, predicting noise folding due to the strong RF input tone.

In a separate application of the block-matrix relation, it is shown that one-sided (or single-sideband) filtering of cyclostationary noise removes cyclostationary components to leave stationary noise. This nonintuitive result is confirmed using the new algorithm and also through extensive Monte Carlo simulations.

The remainder of the paper is organized as follows. In Section II, the need for cyclostationary analysis is motivated with a simple example, and the concept of harmonic power spectral densities introduced. The cyclostationary formulation, block-matrix relation, and algorithm for large circuits are then presented in Section III. In Section IV, the effect of single-sideband filtering of cyclostationary noise is investigated. In Section V, the new algorithm is verified against Monte Carlo simulations, and circuit examples presented.

II. CYCLOSTATIONARY NOISE AND HPSD'S

The circuit of Fig. 1 consists of a mixer, followed by a bandpass filter, followed by another mixer. This is a simplification of, e.g., the bias-dependent noise generation mechanism in
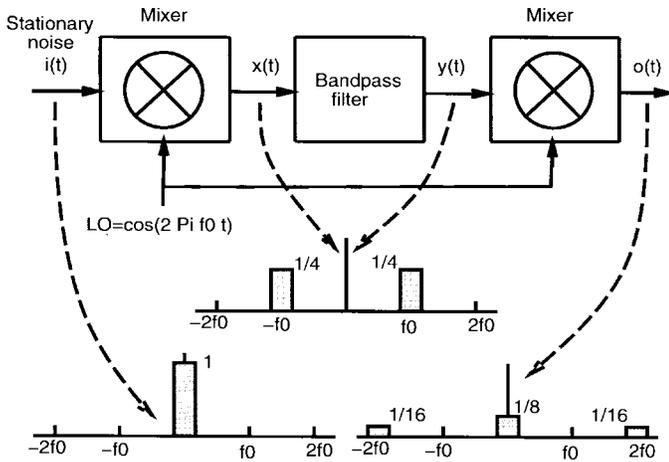
Fig. 1. Mixer-filter-mixer circuit: naïve analysis.

semiconductor devices [6]. Both mixers multiply their inputs by a local oscillator (LO) of frequency f_0, i.e., by $\cos(2\pi f_0 t)$. The bandpass filter is centered around f_0 and has a bandwidth of $B \ll f_0$. The circuit itself is noiseless, but the input to the first mixer is stationary band-limited noise with two-sided bandwidth B.

A naïve attempt to determine the output noise power would consist of the following analysis, illustrated in Fig. 1. The first mixer shifts the input noise spectrum by $\pm f_0$ and scales it by 1/4. The resulting spectrum is multiplied by the squared magnitude of the filter's transfer function. Since this spectrum falls within the passband of the filter, it is not modified. Finally, the second mixer shifts the spectrum again by $\pm f_0$ and scales it by 1/4, resulting in the spectrum with three components shown in the figure. The total noise power at the output, i.e., the area under the spectrum, is 1/4 that at the input.

This common but simplistic analysis is inconsistent with the following alternative argument. Note that the bandpass filter, which does not modify the spectrum of its input, can be ignored. The input then passes through only the two successive mixers, resulting in the output noise voltage $o(t) = i(t) \cos^2(2\pi f_0 t)$. The output power is

$$o^2(t) = i^2(t) \left[\frac{3}{8} + \frac{\cos(2\pi 2 f_0 t) + \cos(2\pi 4 f_0 t)}{2} \right].$$

The average output power consists of only the $3/8 i^2(t)$ term, since the cosine terms time-average to zero. Hence, the average output power is 3/8 of the input power, 50% more than that predicted by the previous naïve analysis. This is, however, the correct result.

The contradiction between the arguments above underscores the need for a more rigorous analysis. Modeling circuit noises as stochastic processes provides the required generality and rigor. Since the local oscillator is periodic, the processes are *cyclostationary* [5], [7], i.e., their statistics vary periodically with time. The autocorrelation function of any cyclostationary process $z(t)$ (defined as $R_{zz}(t, \tau) = E[z(t) z(t+\tau)]$, with $E[\cdot]$ denoting expectation) can be expanded in a Fourier series in t

$$R_{zz}(t, \tau) = \sum_{i=-\infty}^{\infty} R_{z_i}(\tau) e^{ji 2\pi f_0 t}. \qquad (1)$$

$R_{z_i}(\tau)$ are termed *harmonic autocorrelation functions*. The periodically time-varying power of $z(t)$ is its autocorrelation function evaluated at $\tau = 0$, i.e., $R_{zz}(t, 0)$. The quantities $R_{z_i}(0)$ represent the harmonic components of the periodically varying power. The average power is simply the value of the dc or *stationary component* $R_{z_0}(0)$.[1] The frequency-domain representation of the harmonic autocorrelations are termed *harmonic power spectral densities* (HPSD's) $S_{z_i}(f)$ of $z(t)$, defined as the Fourier transforms

$$S_{z_i}(f) = \int_{-\infty}^{\infty} R_{z_i}(\tau) e^{-j\pi f \tau} \, d\tau. \qquad (2)$$

Equations can be derived that relate the HPSD's at the inputs and outputs of various circuit blocks. By solving these equations, any HPSD's in the circuit can be determined.

Consider, for example, the circuit in Fig. 1. The input and output HPSD's of a perfect cosine mixer with unit amplitude can be shown [8] to be related by

$$S_{v_k}(f) = \frac{S_{u_{k-2}}(f - f_0)}{4} + \frac{S_{u_k}(f - f_0) + S_{u_k}(f + f_0)}{4} + \frac{S_{u_{k+2}}(f + f_0)}{4} \qquad (3)$$

(u and v denoting the input and output, respectively). The HPSD relation for a filter with transfer function $H(f)$ is [8]

$$S_{v_k}(f) = H(-f) H(f + k f_0) S_{u_k}(f). \qquad (4)$$

The HPSD's of the circuit are illustrated in Fig. 2. Since the input noise $i(t)$ is stationary, its only nonzero HPSD is the stationary component $S_{i_0}(f)$, assumed to be unity in the frequency band $[-B/2, B/2]$, as shown. From (3) applied to the first mixer, *three* nonzero HPSD's (S_{x_0}, S_{x_2}, and $S_{x_{-2}}$, shown in the figure) are obtained for $x(t)$. These are generated by shifting the input PSD by $\pm f_0$ and scaling by 1/4; in contrast to the naïve analysis, the stationary HPSD is not the only spectrum used to describe the upconverted noise. From (4), it is seen that the ideal bandpass filter propagates the three HPSD's of $x(t)$ unchanged to $y(t)$. Through (3), the second mixer generates five nonzero HPSD's, of which only the stationary component $S_{o_0}(f)$ is shown in the figure. This is obtained by scaling and shifting not only the stationary HPSD of $y(t)$, but also the cyclostationary HPSD's, which in fact contribute an extra 1/4 to the lobe centered at zero. The average output noise (the shaded area under $S_{o_0}(f)$) equals 3/8 of the input noise.

This simple example illustrates how the HPSD approach can be used to analyze RF noise rigorously yet conveniently. HPSD's are in fact a powerful tool: incorporating a nonideal filter in Fig. 1 is simple using (4), and noise propagation through circuits is easy to visualize; this can result in insights that are otherwise difficult to obtain (e.g., see Section IV). The formulation is useful not only for hand calculations and proofs, but also for simulating large circuits, since the HPSD's of circuit unknowns obey a block-matrix relation. This equation, together with an efficient algorithm to compute it for large circuits, is described in Section III.

[1] *Stationary* processes are a special case of cyclostationary processes, where the autocorrelation function (hence the power) is independent of the time t; it follows that $R_{z_i}(\tau) \equiv 0$ if $i \neq 0$.
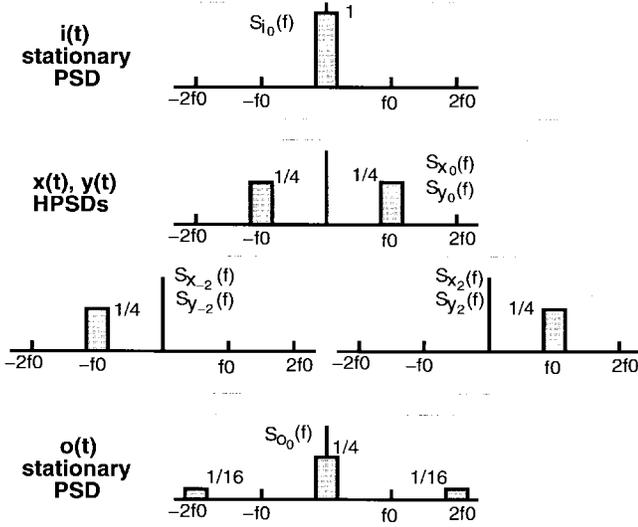
Fig. 2. HPSD's of mixer-filter-mixer circuit.

III. EFFICIENT CYCLOSTATIONARY NOISE COMPUTATION ALGORITHM

The equations of any nonlinear circuit can be expressed in the form

$$\dot{q}(x(t)) + f(x(t)) + b(t) + Au(t) = 0 \qquad (5)$$

where $x(t)$ are the time-domain circuit variables or unknowns, $b(t)$ is a vector of large-signal excitations, and f and q represent the "resistive" and "dynamic" elements of the circuit, respectively. The last term $Au(t)$ represents "small" perturbations to the system, e.g., from noise sources in devices. All these quantities are vectors of dimension n. $u(t)$ has dimension m, representing the number of noise sources in the circuit. A is an incidence matrix of size $n \times m$ which describes how these noise sources are connected to the circuit.

Since the noise sources $u(t)$ are small, their effects can be analyzed by perturbing the noise-free solution of the circuit. Let $x^*(t)$ represent the large signal solution of (5) with $u(t)$ set to zero. Performing a time-varying linearization of (5) about x^*, the following linearized small-signal differential equation is obtained:

$$C(t)\dot{x} + G(t)x + Au(t) = 0. \qquad (6)$$

$x(t)$ in (6) now represents the small-signal deviations of the perturbed solution of (5) from the noise-free solution x^*. $C(t)$ and $G(t)$ are the derivative matrices of $f(\cdot)$ and $q(\cdot)$.

Equation (6) is a linear differential equation with time-varying coefficients. It therefore describes a linear time-varying (LTV) system with input $u(t)$ and output $x(t)$. The LTV system is characterized completely by its time-varying impulse response (or kernel) $h(t_2, t_1)$, an $n \times m$ matrix. The dependence of h on $C(t)$, $G(t)$, and A will be examined in Section III-B; the propagation of noise through LTV systems is analyzed next.

A. Propagation of Noise Through a Linear Time-Varying (LTV) System

The input–output relation of the LTV system described by (6) is

$$x(t_2) = \int_{-\infty}^{\infty} h(t_2, t_1)u(t_1)\,dt_1. \qquad (7)$$

The objective of this section is to obtain a relation between the statistics of u and x if they are stochastic processes. Assuming that they are nonstationary processes, their covariance matrices are defined as [5], [7], [9]

$$R_{pp}(t_1, t_2) = E\big[p(t_1)p^T(t_2)\big] \qquad (8)$$

where p is u or x. A straightforward analysis establishes the following relation between R_{xx} and R_{uu}:

$$R_{xx}(t_1, t_2) = \int_{-\infty}^{\infty}\!\!\int_{-\infty}^{\infty} h(t_1, \tau_1)R_{uu}(\tau_1, \tau_2)h^T(t_2, \tau_2)d\tau_1 d\tau_2. \qquad (9)$$

Most nonlinear systems of interest involve periodic waveforms. If $x^*(t)$, the unperturbed solution of (5), is periodic with period T, then $C(t)$ and $G(t)$ of (6) are also T-periodic. Hence $h(t_2, t_1)$ describes a linear *periodic* time-varying (LPTV) system, and $h(t_2, t_1)$ is periodic with respect to displacements of T in both its arguments, i.e.,

$$h(t_2 + T, t_1 + T) = h(t_2, t_1). \qquad (10)$$

The periodicity of h implies that it can be expanded in a Fourier series

$$h(t_2, t_1) = \sum_{i=-\infty}^{\infty} h_i(t_2 - t_1)e^{ji\omega_0 t_2}, \quad \omega_0 = \frac{2\pi}{T}. \qquad (11)$$

h_i in the above equation are functions of one variable and will be referred to as the *harmonic impulse responses* of the LPTV system. Moreover, their Fourier transforms will be denoted by H_i and referred to as the *harmonic transfer functions* of the LPTV system, i.e.,

$$H_i(\omega) = \int_{-\infty}^{\infty} h_i(t)e^{-j\omega t}\,dt. \qquad (12)$$

Next, two-dimensional power spectral densities are defined by taking two-dimensional Fourier transforms of R_{xx} and R_{uu} [5], [9]

$$S_{pp}(\omega_1, \omega_2) = \int_{-\infty}^{\infty}\!\!\int_{-\infty}^{\infty} R_{pp}(t_1, t_2)e^{-j\omega_1 t_1}e^{-j\omega_2 t_2}dt_1 dt_2. \qquad (13)$$

By Fourier transforming (9) and using the definitions in (12)–(13), an expression relating S_{xx} and S_{uu} is obtained

$$\begin{aligned} S_{xx}&(\omega_1, \omega_2) \\ &= \sum_{i,k=-\infty}^{\infty} H_k(\omega_1 - k\omega_0)S_{uu}(\omega_1 - k\omega_0, \omega_2 - i\omega_0) \\ &\qquad H_i^T(\omega_2 - i\omega_0). \end{aligned} \qquad (14)$$

The assumption that both input and output noises are *cyclostationary* is now introduced. The cyclostationary assumption

implies that R_{xx} and R_{uu} do not change if T is added to both arguments, i.e.,

$$R_{pp}(t_1 + T, t_2 + T) = R_{pp}(t_1, t_2). \qquad (15)$$

Hence both can be expressed as Fourier series

$$R_{pp}(t_1, t_2) = \sum_{i=-\infty}^{\infty} R_{pp_i}(t_2 - t_1)e^{ji\omega_0 t_2}. \qquad (16)$$

R_{xx_i} and R_{uu_i} are functions of one variable and will be referred to as the *harmonic covariances* of the output and input noise, respectively. Their (one-dimensional) Fourier transforms will be denoted by S_{xx_i} and S_{uu_i} and referred to as *harmonic PSD's* or *HPSD's*, i.e.,

$$S_{pp_i}(\omega) = \int_{-\infty}^{\infty} R_{pp_i}(t)e^{-j\omega t}\, dt. \qquad (17)$$

The harmonic covariances and PSD's have simple physical interpretations. $R_{xx}(t,t)$ represents the time-varying power of the cyclostationary noise; hence by (17), $R_{xx_i}(0)$ (the harmonic covariances evaluated at zero) represent the Fourier components of the periodically varying noise power. In particular, $R_{xx_0}(0)$ is the average value, or stationary component, of the power. From the definition of the harmonic PSD's, it follows that the harmonic covariances evaluated at zero are equal to the corresponding harmonic PSD's integrated over the entire frequency axis. Hence $S_{xx_0}(\omega)$ integrated equals the stationary component of the output noise power. S_{xx_0} and S_{uu_0} will be therefore be termed *stationary PSD's*.

When the T-periodic assumption of (15) and the definitions of (16) and (17) are applied to (13), the following form is obtained for the two-dimensional power spectral densities S_{xx} and S_{uu} [5]:

$$S_{pp}(\omega_1, \omega_2) = \sum_{i=-\infty}^{\infty} S_{pp_i}(-\omega_1)\delta(\omega_1 + \omega_2 - i\omega_0). \qquad (18)$$

Using (18), the relation between the two-dimensional power spectral densities [(14)] is rewritten in terms of the (one-dimensional) harmonic PSD's S_{xx_i} and S_{uu_i}

$$S_{xx_l}(-\omega) = \sum_{k,i=-\infty}^{\infty} \frac{H_i(\omega - i\omega_0)S_{uu_k}(-\omega + i\omega_0)}{H_{l-(i+k)}^T(-\omega + (i+k)\omega_0)}. \qquad (19)$$

Equation (19), relating the harmonic PSD's of the input and output noise, is an extension to cyclostationary noise inputs of a similar equation by Ström and Signell [5]. An interesting and useful observation about (19) is that the output harmonic l appears only in the last term $H_{l-(j+k)}^T$. This suggests that (19) can be written in block matrix form. It can be verified by direct multiplication that (19) is equivalent to the following block matrix equation:

$$\mathcal{S}_{xx}(\omega) = \mathcal{H}(\omega)\mathcal{S}_{uu}(\omega)\mathcal{H}^*(\omega) \qquad (20)$$

where $\mathcal{H}^*$ denotes the Hermitian of $\mathcal{H}$. $\mathcal{S}_{xx}$, $\mathcal{S}_{uu}$, and $\mathcal{H}$ are block matrices with an infinite number of blocks, shown at the bottom of the page in (21)–(23) (denoting $w + k\omega_0$ by w^k for conciseness).

Equation (20) expresses the relation between the output and input harmonic PSD's compactly using block matrices. Note from (22) that the output harmonic PSD's evaluated

$$\mathcal{H}(\omega) = \begin{bmatrix} & \vdots & \vdots & \vdots & \vdots & \vdots & \\ \cdots & H_0(\omega^2) & H_1(\omega^1) & H_2(\omega^0) & H_3(\omega^{-1}) & H_4(\omega^{-2}) & \cdots \\ \cdots & H_{-1}(\omega^2) & H_0(\omega^1) & H_1(\omega^0) & H_2(\omega^{-1}) & H_3(\omega^{-2}) & \cdots \\ \cdots & H_{-2}(\omega^2) & H_{-1}(\omega^1) & H_0(\omega^0) & H_1(\omega^{-1}) & H_2(\omega^{-2}) & \cdots \\ \cdots & H_{-3}(\omega^2) & H_{-2}(\omega^1) & H_{-1}(\omega^0) & H_0(\omega^{-1}) & H_1(\omega^{-2}) & \cdots \\ \cdots & H_{-4}(\omega^2) & H_{-3}(\omega^1) & H_{-2}(\omega^0) & H_{-1}(\omega^{-1}) & H_0(\omega^{-2}) & \cdots \\ & \vdots & \vdots & \vdots & \vdots & \vdots & \end{bmatrix} \qquad (21)$$

$$\mathcal{S}_{xx}(\omega) = \begin{bmatrix} & \vdots & \vdots & \vdots & \vdots & \vdots & \\ \cdots & S_{xx_0}(-\omega^2) & S_{xx_1}(-\omega^2) & S_{xx_2}(-\omega^2) & S_{xx_3}(-\omega^2) & S_{xx_4}(-\omega^2) & \cdots \\ \cdots & S_{xx_{-1}}(-\omega^1) & S_{xx_0}(-\omega^1) & S_{xx_1}(-\omega^1) & S_{xx_2}(-\omega^1) & S_{xx_3}(-\omega^2) & \cdots \\ \cdots & S_{xx_{-2}}(-\omega^0) & S_{xx_{-1}}(-\omega^0) & S_{xx_0}(-\omega^0) & S_{xx_1}(-\omega^0) & S_{xx_2}(-\omega^0) & \cdots \\ \cdots & S_{xx_{-3}}(-\omega^{-1}) & S_{xx_{-2}}(-\omega^{-1}) & S_{xx_{-1}}(-\omega^{-1}) & S_{xx_0}(-\omega^{-1}) & S_{xx_1}(-\omega^{-1}) & \cdots \\ \cdots & S_{xx_{-4}}(-\omega^{-2}) & S_{xx_{-3}}(-\omega^{-2}) & S_{xx_{-2}}(-\omega^{-2}) & S_{xx_{-1}}(-\omega^{-2}) & S_{xx_0}(-\omega^{-2}) & \cdots \\ & \vdots & \vdots & \vdots & \vdots & \vdots & \end{bmatrix} \qquad (22)$$

$$\mathcal{S}_{uu}(\omega) = \begin{bmatrix} & \vdots & \vdots & \vdots & \vdots & \vdots & \\ \cdots & S_{uu_0}(-\omega^2) & S_{uu_1}(-\omega^2) & S_{uu_2}(-\omega^2) & S_{uu_3}(-\omega^2) & S_{uu_4}(-\omega^2) & \cdots \\ \cdots & S_{uu_{-1}}(-\omega^1) & S_{uu_0}(-\omega^1) & S_{uu_1}(-\omega^1) & S_{uu_2}(-\omega^1) & S_{uu_3}(-\omega^2) & \cdots \\ \cdots & S_{uu_{-2}}(-\omega^0) & S_{uu_{-1}}(-\omega^0) & S_{uu_0}(-\omega^0) & S_{uu_1}(-\omega^0) & S_{uu_2}(-\omega^0) & \cdots \\ \cdots & S_{uu_{-3}}(-\omega^{-1}) & S_{uu_{-2}}(-\omega^{-1}) & S_{uu_{-1}}(-\omega^{-1}) & S_{uu_0}(-\omega^{-1}) & S_{uu_1}(-\omega^{-1}) & \cdots \\ \cdots & S_{uu_{-4}}(-\omega^{-2}) & S_{uu_{-3}}(-\omega^{-2}) & S_{uu_{-2}}(-\omega^{-2}) & S_{uu_{-1}}(-\omega^{-2}) & S_{uu_0}(-\omega^{-2}) & \cdots \\ & \vdots & \vdots & \vdots & \vdots & \vdots & \end{bmatrix} \qquad (23)$$

at $\omega (=\omega^0)$ are given by the central block-row of $\mathcal{S}_{xx}$. The HPSD's of the self- and cross-powers of the pth output x_p are available in the pth row of this block. Denote the transpose of this row by $\mathcal{S}^T_{xx_{(\cdot,0)(\cdot,p)}}$; this is obtained by transposing (20) and postmultiplying by a unit block-vector E_0 followed by the pth unit vector e_p

$$\mathcal{S}^T_{xx_{(\cdot,0)(\cdot,p)}}(\omega) = \bar{\mathcal{H}}(\omega)\mathcal{S}^T_{uu}(\omega)\mathcal{H}^T(\omega)E_0 e_p \qquad (24)$$

where

$$E_0 = \begin{bmatrix} \vdots \\ 0 \\ 0 \\ I_{n\times n} \\ 0 \\ 0 \\ \vdots \end{bmatrix} \leftarrow \text{0th block}, \qquad e_p = \begin{bmatrix} 0 \\ \vdots \\ \vdots \\ 1 \\ \vdots \\ 0 \end{bmatrix} \begin{matrix} \leftarrow \text{1st entry} \\ \\ \\ \leftarrow p\text{th entry} \\ \\ \leftarrow n\text{th entry} \end{matrix} \qquad (25)$$

where $I_{n\times n}$ represents the $n \times n$ identity matrix. Note that $E_0 e_p$ is a vector. Hence the computation of $\mathcal{S}^T_{xx_{(\cdot,0)(\cdot,p)}}(\omega)$ in (24) can be performed by matrix-vector products with the block matrices $\mathcal{H}^T$, $\mathcal{S}^T_{uu}$, and $\bar{\mathcal{H}}$. Despite the fact that these matrices are, in general, dense, products with them can be performed efficiently, as discussed next in Sections III-B and III-C.

B. Fast Application of $\mathcal{H}^T$ and $\bar{\mathcal{H}}$ Exploiting Harmonic Balance

To apply $\mathcal{H}^T$ and $\bar{\mathcal{H}}$ efficiently to a vector, it is necessary to represent $\mathcal{H}$ in terms of $C(t)$, $G(t)$, and A [refer to (6)]. Since $C(t)$ and $G(t)$ are T-periodic, they are expanded in Fourier series

$$C(t) = \sum_{i=-\infty}^{\infty} C_i e^{ji\omega_0 t}, \quad G(t) = \sum_{i=-\infty}^{\infty} G_i e^{ji\omega_0 t}. \qquad (26)$$

The Fourier coefficients C_i and G_i will be referred to as the harmonics of $C(t)$ and $G(t)$, respectively. It can be shown [10] that $\mathcal{H}$ can be expressed in terms of these harmonics as

$$\mathcal{H}(\omega) = J^{-1}(\omega)\mathcal{A}, \quad J(\omega) = \mathcal{G} + j\Omega(\omega)\mathcal{C} \qquad (27)$$

where

$$\mathcal{C} = \begin{bmatrix} & \vdots & \vdots & \vdots & \vdots & \vdots & \\ \cdots & C_0 & C_{-1} & C_{-2} & C_{-3} & C_{-4} & \cdots \\ \cdots & C_1 & C_0 & C_{-1} & C_{-2} & C_{-3} & \cdots \\ \cdots & C_2 & C_1 & C_0 & C_{-1} & C_{-2} & \cdots \\ \cdots & C_3 & C_2 & C_1 & C_0 & C_{-1} & \cdots \\ \cdots & C_4 & C_3 & C_2 & C_1 & C_0 & \cdots \\ & \vdots & \vdots & \vdots & \vdots & \vdots & \end{bmatrix} \qquad (28)$$

$$\mathcal{G} = \begin{bmatrix} & \vdots & \vdots & \vdots & \vdots & \vdots & \\ \cdots & G_0 & G_{-1} & G_{-2} & G_{-3} & G_{-4} & \cdots \\ \cdots & G_1 & G_0 & G_{-1} & G_{-2} & G_{-3} & \cdots \\ \cdots & G_2 & G_1 & G_0 & G_{-1} & G_{-2} & \cdots \\ \cdots & G_3 & G_2 & G_1 & G_0 & G_{-1} & \cdots \\ \cdots & G_4 & G_3 & G_2 & G_1 & G_0 & \cdots \\ & \vdots & \vdots & \vdots & \vdots & \vdots & \end{bmatrix} \qquad (29)$$

$$\Omega(\omega) = \begin{bmatrix} \ddots & & & & \\ & \omega^{-1}I & & & \\ & & \omega^0 I & & \\ & & & \omega^1 I & \\ & & & & \ddots \end{bmatrix} \qquad (30)$$

$$\mathcal{A} = \begin{bmatrix} \ddots & & & & & & \\ & A & & & & & \\ & & A & & & & \\ & & & A & & & \\ & & & & A & & \\ & & & & & A & \\ & & & & & & \ddots \end{bmatrix}. \qquad (31)$$

$J(\omega)$ is known as the *conversion matrix* [10] of the circuit; $J(0)$ is the Jacobian matrix of the harmonic balance equations at the circuit's steady state x^*.

For numerical computation, the infinite block matrices in (21)–(23) and (28)–(31) are truncated to a finite number of blocks $N = 2M + 1$. M is the largest positive harmonic considered. For the purposes of the analysis, it is assumed that no significant harmonic PSD of degree greater than $M/2$ exists for the input noise $u(t)$ or the output noise $x(t)$. Since the energy content of the ith harmonic is always a diminishing function of i in practical RF circuits, a value for M can always be found satisfying this assumption.

With this assumption, it can be shown that the Toeplitz block structure in the above matrices can be approximated by *circulant* block structure without loss of accuracy in the matrix-vector product. For example, $\mathcal{C}$ truncated to $N = 7$ blocks can be approximated by $\overset{\circ}{\mathcal{C}}$, given by

$$\overset{\circ}{\mathcal{C}} = \begin{bmatrix} C_0 & C_{-1} & C_{-2} & C_{-3} & C_3 & C_2 & C_1 \\ C_1 & C_0 & C_{-1} & C_{-2} & C_{-3} & C_3 & C_2 \\ C_2 & C_1 & C_0 & C_{-1} & C_{-2} & C_{-3} & C_3 \\ C_3 & C_2 & C_1 & C_0 & C_{-1} & C_{-2} & C_{-3} \\ C_{-3} & C_3 & C_2 & C_1 & C_0 & C_{-1} & C_{-2} \\ C_{-2} & C_{-3} & C_3 & C_2 & C_1 & C_0 & C_{-1} \\ C_{-1} & C_{-2} & C_{-3} & C_3 & C_2 & C_1 & C_0 \end{bmatrix}. \qquad (32)$$

Note that the fourth, fifth, and sixth sub- and super-diagonals of $\overset{\circ}{\mathcal{C}}$ differ from those of $\mathcal{C}$ truncated to seven blocks. Matrix-vector products with $\overset{\circ}{\mathcal{C}}$ and the truncated $\mathcal{C}$, however, produce identical results up to the first harmonic location if the vector being multiplied contains no significant components in the second and third harmonic locations.

The utility of the circulant approximation is that it enables $\overset{\circ}{\mathcal{C}}$ and $\overset{\circ}{\mathcal{G}}$ to be decomposed into products of sparse block-diagonal matrices, permutations, and Fourier transform (DFT) matrices [11]–[13]. This enables matrix-vector products with $\overset{\circ}{\mathcal{C}}$ and $\overset{\circ}{\mathcal{G}}$ to be performed as a sequence of products with sparse block-diagonal matrices ($O(nN)$ operations), permutations (no cost), and Fourier transforms ($O(nN \log N)$ operations); hence the overall computation is $O(nN \log N)$. Further, since only the sparse block-diagonal matrices need to be stored, the memory requirement is $O(nN)$. Note that $\Omega(\omega)$ is a diagonal matrix with *a priori* known entries ω^k, hence its application to a vector is $O(nN)$ in computational cost, with

no memory required for its storage. The net effect of the circulant approximation, therefore, is that $J(\omega)$ can be applied to a vector in $O(nN \log N)$ computation and $O(nN)$ memory.

From (27), it follows that to obtain the required matrix-vector product with $\mathcal{H}(\omega)$, matrix-vector products with $\mathcal{A}$ and $J^{-1}(\omega)$ are necessary. Since $\mathcal{A}$ is a sparse block-diagonal matrix with identical blocks A (the noise source incidence matrix), it can be applied in $O(nN)$ time and $O(n)$ memory. *Iterative linear solvers* [14], [15] can obtain the matrix-vector product with J^{-1} using only matrix-vector products with J. The use of iterative linear techniques, together with the decomposition of J allowing its application in $O(nN \log N)$ time, is the key to the fast harmonic balance algorithms of Rösch [12], [13], [16] and Melville *et al.* [11]. With suitable preconditioning included in the iterative solution, the number of J-vector products required to compute a J^{-1}-vector product is small and approximately independent of the size of J. Hence the J^{-1}-vector product can be computed in approximately $O(nN \log N)$ time and $O(nN)$ memory, leading to the same computation and memory requirements for the desired product with $\mathcal{H}$.

From Section III-A, products are required with $\mathcal{H}^T$ and $\bar{\mathcal{H}}$ for cyclostationary noise computation. Application of $\mathcal{H}^T$ is carried out using the same decomposition and iterative linear methods as for $\mathcal{H}$, but using transposes of the matrices involved. The product with $\bar{\mathcal{H}}$ is carried out using the relation $\bar{\mathcal{H}}z = \overline{\mathcal{H}\bar{z}}$.

C. Fast Application of $\mathcal{S}_{uu}^T$

The principal sources of noise in circuits are thermal, shot, and flicker $(1/f)$ noises from devices. When the linearized small-signal circuit [(6)] is time-invariant (i.e., the circuit is in dc steady state), these noise sources are stationary stochastic processes with known power spectral densities. Thermal and shot noises are white, i.e., their PSD values are constant, independent of frequency; flicker noise PSD's exhibit a $\frac{1}{f}$ variation with frequency. The expressions for the power spectral densities of these noise sources (see, e.g., Van der Ziel [17]) typically involve some component of the dc solution; for example, the PSD of the shot noise current $u_D(t)$ across a diode's p-n junction is proportional to the dc current I_D through the junction, i.e.,

$$S_{u_D u_D}(\omega) = 2qI_D \tag{33}$$

where $S_{u_D u_D}(\omega)$ is the (stationary) PSD of the shot noise and q is the electronic charge.

From the viewpoint of second-order statistics, the diode's shot noise is equivalent to the hypothetical process generated by multiplying a white noise process $w(t)$ of PSD value $2q$ by a constant factor of $\sqrt{I_D}$

$$u_D(t) = \sqrt{I_D}w(t), \quad S_{ww}(\omega) = 2q. \tag{34}$$

For this reason, shot noise is often said, in a loose sense, to be proportional to $\sqrt{I_D}$.

For circuits operating in dc steady state, expressions for PSD's of stationary noise generators are well established from theoretical considerations and/or through measurement. For circuits operating in time-varying steady state, unfortunately, there are as yet no stochastic models for the nonstationary noise generation process that are well established. Nevertheless, there is general consensus that for white processes like shot and thermal noise, the time variation is generated by modulating stationary white noise by the (deterministic) time-varying large-signal steady state. For the diode shot noise example above, (34) generalizes to

$$u_D(t) = \sqrt{I_D(t)}w(t), \quad S_{ww}(\omega) = 2q \tag{35}$$

where $I_D(t)$ is a time-varying waveform. Arguments supporting this deterministic modulation model are based on the short-term nature of the autocorrelations of thermal and shot noise; see, e.g., [3], [18], and [19].

For noise with long-term correlations (notably flicker noise), there is a general belief that the above deterministic-modulation-of-stationary-noise model is inadequate (e.g., [20]). The physical processes responsible for generating long-term noise correlations, it is argued, are themselves modified by the large-signal waveforms which change on a relatively faster scale. Unfortunately, neither theoretical analyses nor experimental data are available at this time, to the authors' knowledge, to aid in formulating a generation mechanism for such noise. In the absence of an established alternative, Demir [18] has used the modulated stationary noise model for analyzing nonstationary flicker noise, and this approach also appears common among designers of RF circuits. The modulated stationary noise model is therefore reluctantly adopted in this work for all cyclostationary noise generators.

Under this noise generation model, the noise input $u(t)$ in (6) can be expressed as

$$u(t) = M(t)u_s(t) \tag{36}$$

where $u_s(t)$ is an m-dimensional vector of stationary noise sources and $M(t)$ is an $m \times m$ diagonal matrix of T-periodic deterministic modulations.

Equation (20) can be used to analyze the relation between statistics of $u(t)$ and $u_s(t)$ by recognizing that (36) represents an LTV system with input $u_s(t)$ and output $u(t)$. The time-varying impulse response of the LTV system is

$$h(t_2, t_1) = \delta(t_2 - t_1)M(t_2) = \sum_{i=-\infty}^{\infty} M_i \delta(t_2 - t_1)e^{ji\omega_0 t_2} \tag{37}$$

where M_i denote the Fourier coefficients of the periodic modulation $M(t)$. The harmonic transfer functions $H_i(\omega)$ are independent of ω and simply equal to M_i. Equation (20) applied to this LTV system results in the following block-matrix relation between the harmonic PSD's of $u(t)$ and $u_s(t)$:

$$\mathcal{S}_{uu}(\omega) = \mathcal{M}\mathcal{S}_{u_s u_s}(\omega)\mathcal{M}^* \tag{38}$$

where $\mathcal{S}_{u_s u_s}(\omega)$ represents the block Toeplitz matrix of the harmonic PSD's of the stationary noise sources. Since the sources are stationary, all their harmonic PSD's are zero except for the stationary PSD $S_{u_s u_{s0}}(\omega)$; hence $\mathcal{S}_{u_s u_s}(\omega)$ is block diagonal with diagonal entries $[\ldots, S_{u_s u_{s0}}(-\omega^2), S_{u_s u_{s0}}(-\omega^1),$

$S_{u_s u_{s0}}(-\omega^0)$, $S_{u_s u_{s0}}(-\omega^{-1})$, $S_{u_s u_{s0}}(-\omega^{-2})$, ...]. $\mathcal{M}$ in (38) is block Toeplitz with M_i in the diagonals

$$\mathcal{M} = \begin{bmatrix} & \vdots & \vdots & \vdots & \vdots & \vdots & \\ \cdots & M_0 & M_1 & M_2 & M_3 & M_4 & \cdots \\ \cdots & M_{-1} & M_0 & M_1 & M_2 & M_3 & \cdots \\ \cdots & M_{-2} & M_{-1} & M_0 & M_1 & M_2 & \cdots \\ \cdots & M_{-3} & M_{-2} & M_{-1} & M_0 & M_1 & \cdots \\ \cdots & M_{-4} & M_{-3} & M_{-2} & M_{-1} & M_0 & \cdots \\ & \vdots & \vdots & \vdots & \vdots & \vdots & \end{bmatrix}. \quad (39)$$

Using (38), the product of $\mathcal{S}_{uu}$ with a vector can be performed through matrix-vector products with the matrices $\mathcal{M}, \mathcal{M}^*$, and $\mathcal{S}_{u_s u_{s0}}$. Products with the block-Toeplitz matrices $\mathcal{M}$ and $\mathcal{M}^*$ can be performed in $O(mN \log N)$ time and $O(mN)$ memory, approximating $\mathcal{M}$ by a block-circulant matrix and applying the same decomposition as for $\mathcal{G}$ in Section III-B. Application of the block-diagonal matrix $\mathcal{S}_{u_s u_s}(\omega)$ is equivalent to N matrix vector products with $S_{u_s u_{s0}}(\cdot)$. If the device noise generators are uncorrelated, $S_{u_s u_{s0}}(\cdot)$ is diagonal; if correlations exist, they are usually between small groups of noise generators, hence $S_{u_s u_{s0}}(\cdot)$ is sparse. In either case, each product with $S_{u_s u_{s0}}(\cdot)$ is $O(m)$ in computation with no storage required. Hence matrix-vector products with $\mathcal{S}_{u_s u_{s0}} O(Nm)$ time and $O(1)$ memory. The overall matrix-vector product with $\mathcal{S}_{uu}$ can therefore be performed in $O(mN \log N)$ time and $O(mN)$ memory.

It should be noted that the noise modulation $M(t)$ can be absorbed into the circuit equations [(5)]. The noise inputs $u(t)$ to the circuit can then be assumed to be stationary without loss of generality. This procedure, however, increases the size of the harmonic balance system for obtaining the steady state x^*. To avoid this and to separate the implementation of the noise algorithm from the harmonic balance steady state algorithm, the formulation of this section is preferred.

IV. BANDPASS FILTERING OF CYCLOSTATIONARY NOISE

Ström and Signell [5] have shown that low-pass filtering of cyclostationary noise results in stationary noise if the bandwidth of the low-pass filter is less than half the frequency of cyclostationarity ω_0. This result has been used by Hull and Meyer [21] to simplify their analysis. In this section, the effect of LTI bandpass filtering on cyclostationary noise is considered. It is shown that if cyclostationary noise is passed through a one-sided (i.e., single-sideband) bandpass filter of bandwidth less than $\omega_0/2$, the output noise is stationary. This result is obtained using a simple visualization of the propagation of harmonic PSD's.

Denote the input noise to a bandpass filter by $n(t)$ and the output noise by $x(t)$. Assume that the input $n(t)$ is cyclostationary with period $T = 2\pi/\omega_0$. Denote the transfer function of the bandpass filter by $H(\omega)$. The relationship between the harmonic PSD's of $n(t)$ and $x(t)$, derived from (24) by using the fact that $\mathcal{H}$ is block diagonal for an LTI network, is

$$S_{xx_i}(\omega) = H(-\omega) S_{nn_i}(\omega) H^T(\omega + i\omega_0). \quad (40)$$
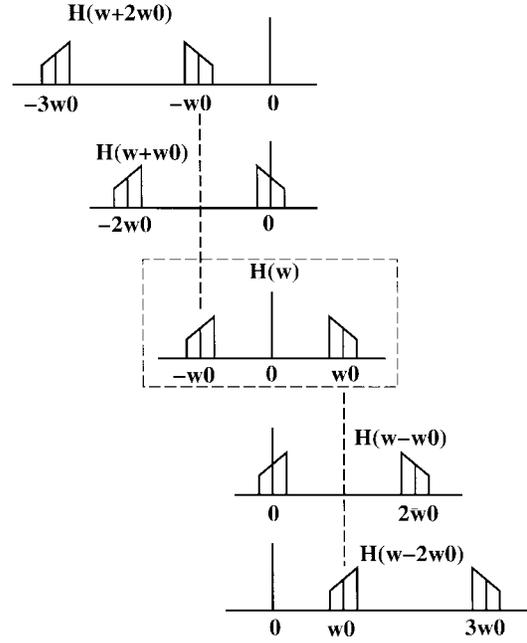
Fig. 3. $H(\omega)$ overlaid with $H(\omega + i\omega_0)$ for $i = 2, 1, -1$ and -2.
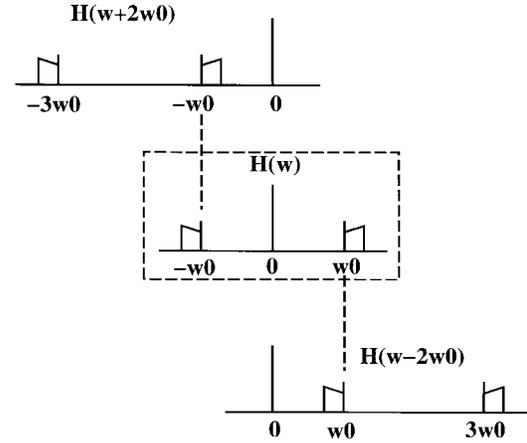
Fig. 4. One-sided $H(\omega)$ overlaid with $H(\omega + i\omega_0)$ for $i = 2$ and -2.

Note that the ith harmonic PSD of the output is determined completely by the corresponding harmonic PSD of the input, shaped by the product of the filter function $H(\omega)$ with a shifted version of itself $H^T(\omega + i\omega_0)$. For the scalar input–output case under consideration, the relation simplifies to

$$S_{xx_i}(\omega) = H(-\omega) H(\omega + i\omega_0) S_{nn_i}(\omega). \quad (41)$$

Since the magnitude of $H(\omega)$ for a real filter is symmetric about zero, $H(-\omega)$ has the same magnitude characteristic as $H(\omega)$. By overlaying the magnitudes of $H(\omega)$ and $H(\omega + i\omega_0)$ for different values of i (illustrated in Fig. 3), it can be seen that the product $H(-\omega) H(\omega + i\omega_0)$ is nonzero only for $i = 0, 2$, and -2 if the bandwidth of $H(\omega)$ is less than $\omega_0/2$. For all other values of i, there is no frequency at which $H(-\omega)$ and $H(\omega + i\omega_0)$ are both nonzero, hence their product is identically zero.

This immediately implies the following.
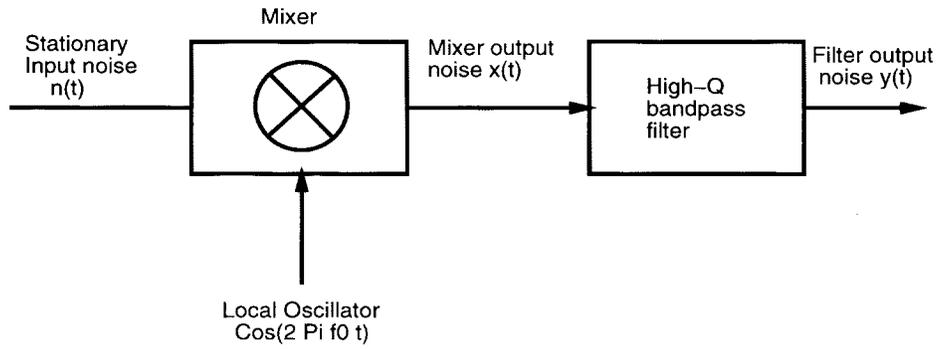
Fig. 5. Mixer and bandpass filter.
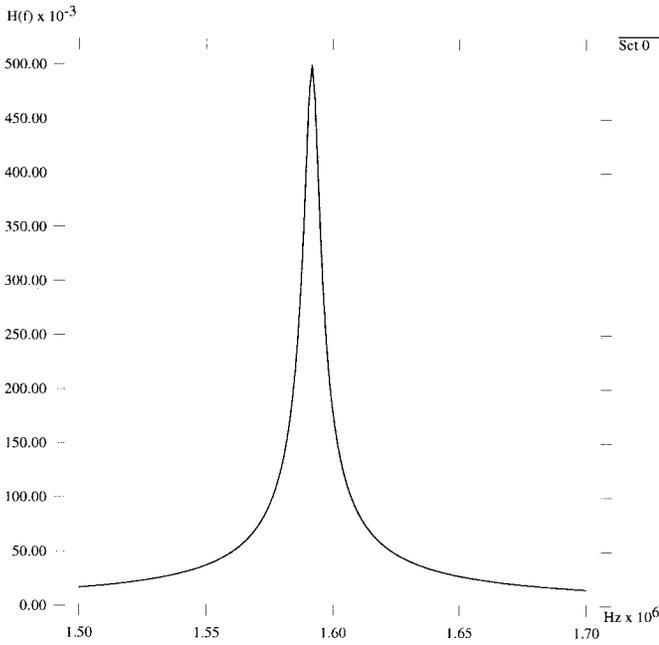
Fig. 6. Bandpass filter characteristic.
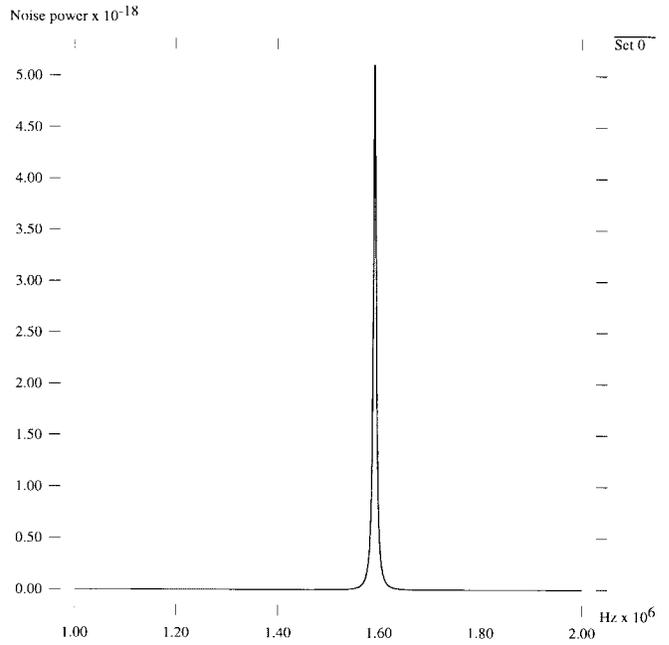
Fig. 7. $S_{yy_0}(f)$ with $f_0 = 1.592$ MHz (double-sideband filtering).

Result 1: Bandpass filtering with bandwidth less than $\omega_0/2$ eliminates all harmonic PSD's except the stationary and second harmonic PSD's.

Moreover, if the bandpass filter is one-sided with respect to ω_0, then the product $H(\omega)H(\omega + i\omega_0)$ is identically zero also for $i = 2$ and -2, as illustrated in Fig. 4. In this case, the bandwidth of the filter can be greater than $\omega_0/2$ but should be less than ω_0. The only nonzero PSD of the output is then the stationary PSD. This implies Result 2.

Result 2: One-sided (or single-sideband) bandpass filtering (with bandwidth less than ω_0) of cyclostationary noise results in stationary output noise.

V. RESULTS

The fast cyclostationary noise algorithm of Section III has been prototyped in a Bell Labs internal simulator. In this section, the algorithm and the single-sideband-filtering results of Section IV are first verified against Monte Carlo noise simulations with 60 000 sample waveforms, to an accuracy of within 2%. Noise analysis results from two circuits are then presented—a mixer excited by a single LO tone, and a large

circuit, consisting of an I-channel buffer and mixer, driven by two strong tones (a signal and an LO).

A. Mixer and Bandpass Filter

Motivated by the result of Section IV, a mixer and bandpass filter circuit (Fig. 5) is analyzed for cyclostationary noise propagation. The mixer is an ideal multiplier that modulates the incoming stationary noise with a deterministic LO oscillator signal $\cos(2\pi f_0 t)$. The filter has a high-Q bandpass characteristic (illustrated in Fig. 6) with a center frequency of approximately 1.592 MHz and a bandwidth of about 50 kHz. The stationary input noise is bandlimited with double-sided bandwidth of about 200 kHz.

Two simulations are carried out, with f_0 set to 1.592 MHz and 1.5 MHz, respectively. In the first situation, the bandpass filter is centered at the LO frequency; in the second, the filter characteristic is offset to the right of the LO frequency, strongly attenuating the lower sideband with respect to f_0 while passing the upper sideband. Harmonic PSD's at all nodes in the circuit were computed over frequencies from 1 MHz to 2 MHz.

Noise power x 10^{-18}
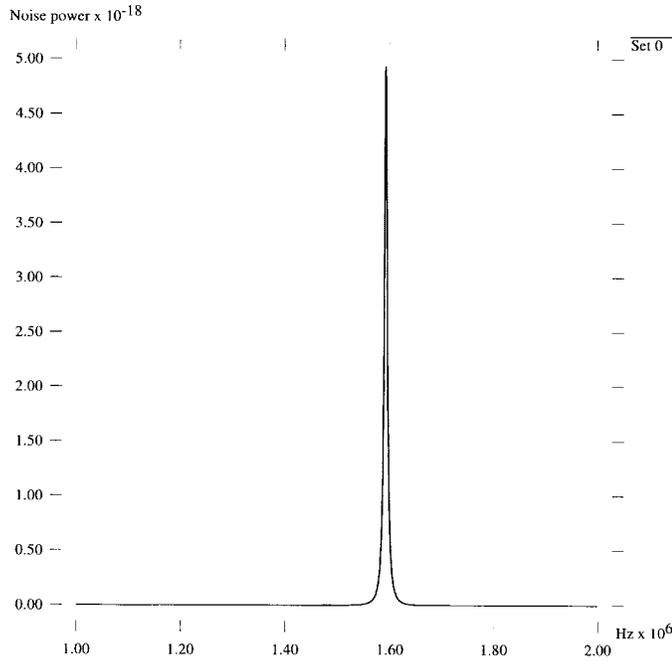
Fig. 8. $S_{yy_{-2}}(f)$ with $f_0 = 1.592$ MHz (double-sideband filtering).

Noise power x 10^{-21}
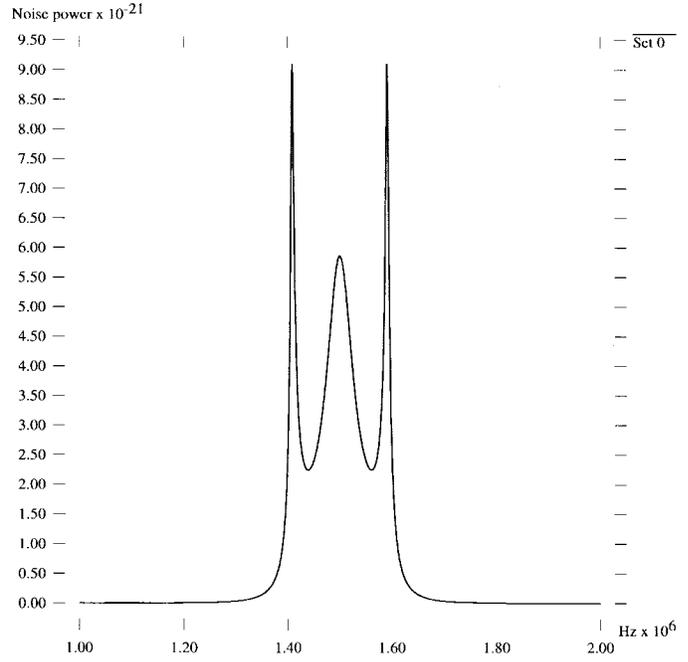
Fig. 10. $S_{yy_{-2}}(f)$ with $f_0 = 1.5$ MHz (single-sideband filtering).

Noise power x 10^{-21}
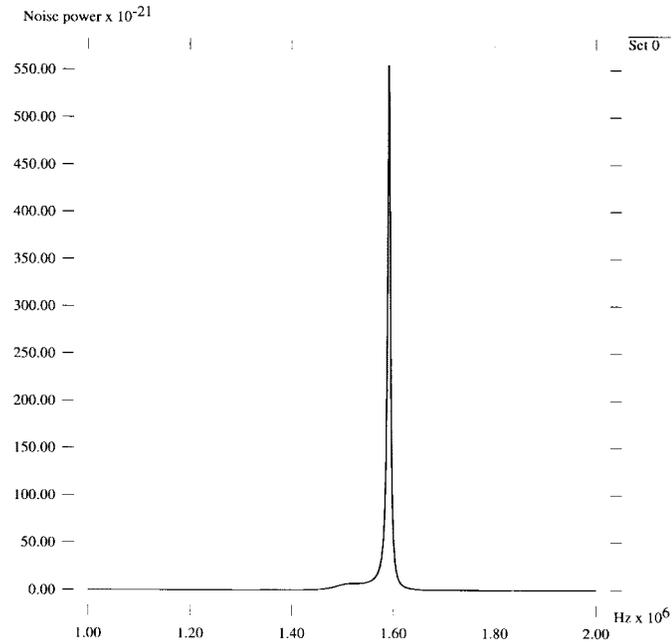
Fig. 9. $S_{yy_0}(f)$ with $f_0 = 1.5$ MHz (single-sideband filtering).

power x 10^{-3}
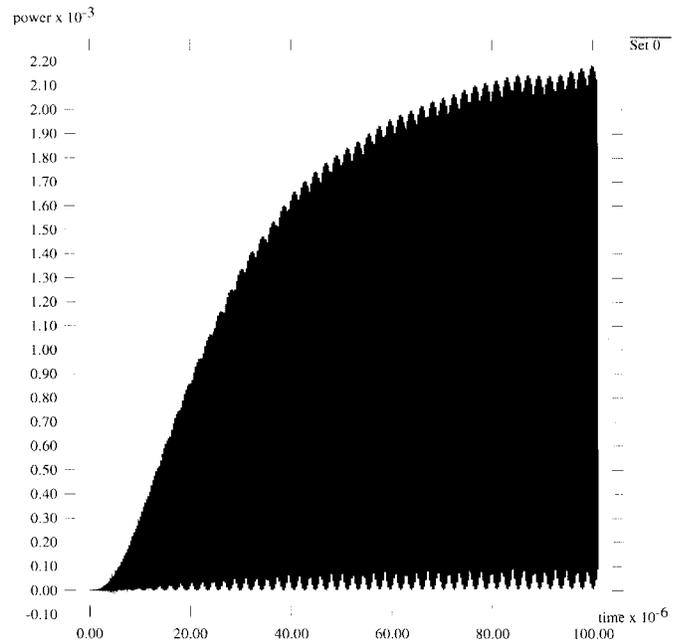
Fig. 11.   Time-varying filtered noise power from Monte Carlo: $f_0 = 1.592$ MHz (double sideband).

Using the results of Section III-A, it can be shown that only the stationary and second harmonic PSD's of the mixer output $x(t)$ are nonzero, related to the PSD of the stationary input by

$$S_{xx_0}(\omega) = \frac{S_{nn_0}(\omega - \omega_0) + S_{nn_0}(\omega - \omega_0)}{4}$$

$$S_{xx_{-2}}(\omega) = \frac{S_{nn_0}(\omega - \omega_0)}{4}, \quad S_{xx_2}(\omega) = \overline{S_{xx_{-2}}(-\omega)}.$$

The stationary and second harmonic PSD's of the filter output $y(t)$ for $f_0 = 1.592$ MHz (double-sideband filtering) are shown in Figs. 7 and 8. It can be seen that both PSD's

have the same magnitude, hence there is a large cyclostationary component in the noise. The same PSD's for the $f_0 = 1.5$ MHz case (single-sideband filtering) are shown in Figs. 9 and 10. The second harmonic PSD can be seen to be about two orders of magnitude smaller than the stationary PSD. Hence the filtered noise is virtually stationary, as predicted in Section IV. The second harmonic PSD is not identically zero because the nonideal single-sideband filter does not perfectly eliminate the lower sideband.
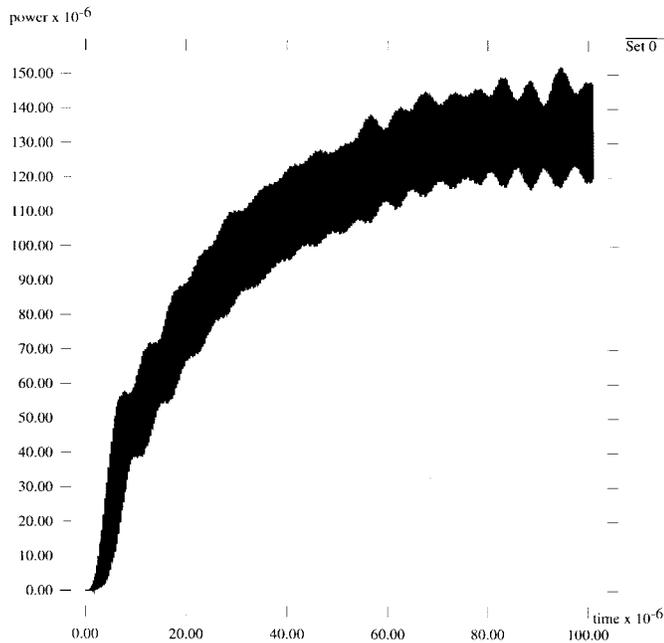
Fig. 12. Time-varying filtered noise power from Monte Carlo: $f_0 = 1.5$ MHz (single sideband).
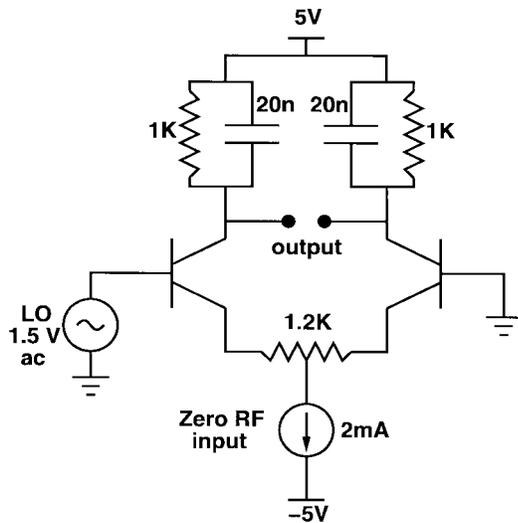
Fig. 13. Mixer cell.

The above results were also verified by simulations using the Monte Carlo method. The nonlinear differential equations of the circuit in Fig. 5 were solved numerically with $60\,000$ samples of the input noise $n(t)$ [22]. The input noise PSD was normalized to one to avoid corruption of the results by numerical noise generated during differential equation solution. The $60\,000$ samples of the mixed and filtered noise $y(t)$ were squared and averaged, on a per-timepoint basis, to obtain the noise power at the output as a function of time. The variation of noise power with time is shown in Figs. 11 and 12 for the double-sideband and single-sideband cases. When analyzed in the time domain, the circuit requires some time to reach large-signal steady state, hence the steady state noise power is approached toward $t = 100$ ms; in contrast, harmonic balance calculates this steady state directly. The

cyclostationarity of the noise in the double-sideband case can be seen from the variation of the power between zero and its maximum value of about 0.0022. In the single-sideband case, the power approaches a steady value of about 130×10^{-6}, with a cyclostationary variation of about 10%. Accounting for the normalization of the input PSD, these values are in excellent agreement with the total integrated noise of $S_{yy_0}(f)$ and $S_{yy_{-2}}(f)$ (Figs. 9 and 10); Monte Carlo simulation results are within 2% of the results produced by the new algorithm.

B. Mixer Analysis

The mixer in Fig. 13 was analyzed for cyclostationary noise to investigate the effect of large-signal LO variations on the output noise. The LO signal of amplitude 1.5 V is applied at the base of the first transistor, as shown. The RF input signal is applied through the current source, which is held at a dc value of 2 mA (i.e., no RF signal) for the noise analysis.

Two simulations were performed: a stationary analysis with no LO present to obtain the noise of the quiescent circuit, and a cyclostationary analysis with the LO amplitude at 1.5 V. The former simulation took a few seconds and the latter (with 25 large-signal harmonics) 40 seconds per frequency point. The stationary PSD is shown in Fig. 14, and some nonstationary HPSD's in Fig. 15.

From Fig. 14, it can be seen that the presence of a large LO signal reduces the average noise power at the output. This is a known property of switching mixers. Fig. 15 shows the first six harmonic PSD's of the noise at the output when the LO is 1.5 V.

From a knowledge of the HPSD's, it is possible to create system-level macromodels for functional blocks like the mixer. All the noise of the circuit can then be concentrated in an equivalent noise source with the same HPSD's. While only the stationary PSD determines the average noise power, the nonstationary HPSD's must be included because they can contribute to the stationary component of some other block, as discussed in Section II.

C. I-Channel Buffer and Mixer Circuit

The next example is a portion of the W2013 RFIC, consisting of an I-channel buffer feeding a mixer. The circuit consisted of about 360 nodes and was excited by two tones—a local oscillator at 178 MHz driving the mixer and a strong RF signal tone at 80 kHz feeding into the I-channel buffer. Two noise analyzes were performed. The first analysis included both LO and RF tones (sometimes called a three-tone noise analysis). The circuit was also analyzed with only the LO tone to determine if the RF signal affects the noise significantly. The two-tone noise simulation, using a total of 525 large-signal mix components, required 300 MB of memory and for each frequency point, took 40 min on an SGI machine (200-MHz R10000 CPU). The one-tone noise simulation, using 45 harmonics, needed 70 MB of memory and took 2 min per point.

The stationary PSD's of the mixer output noise for the two simulations are shown in Fig. 16. It can be seen that the presence of the large RF signal increases the noise by

Stationary PSDs for no LO and LO=1.5V
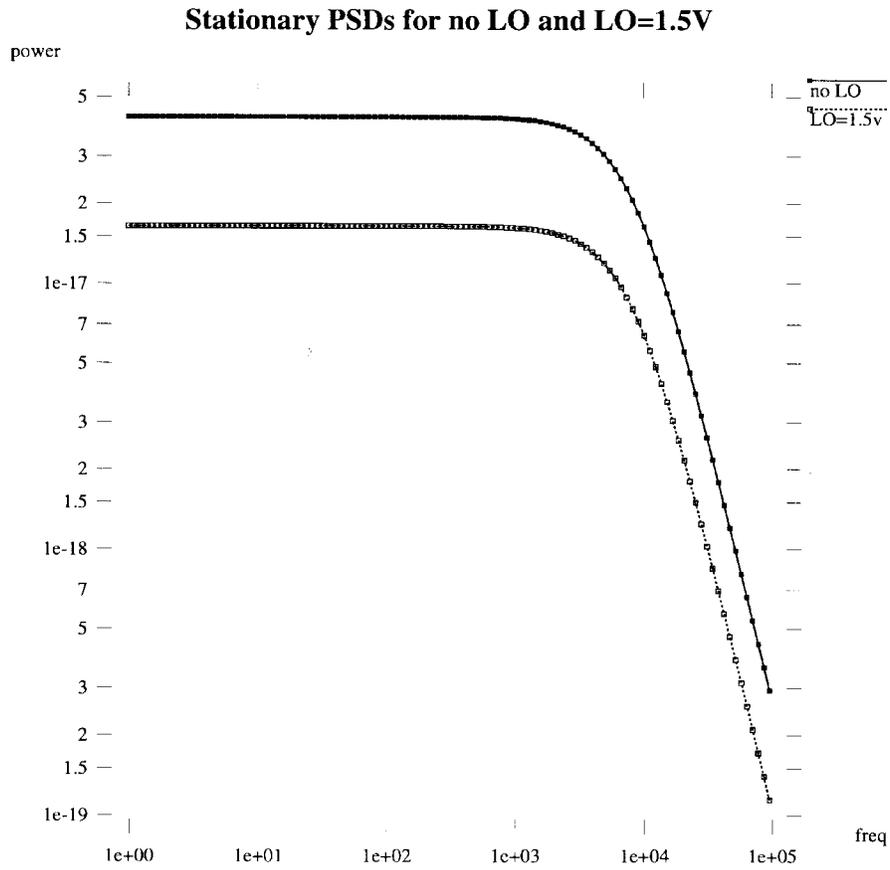
Fig. 14.   Mixer: stationary PSD at output.

Harmonic PSDs for LO=1.5V
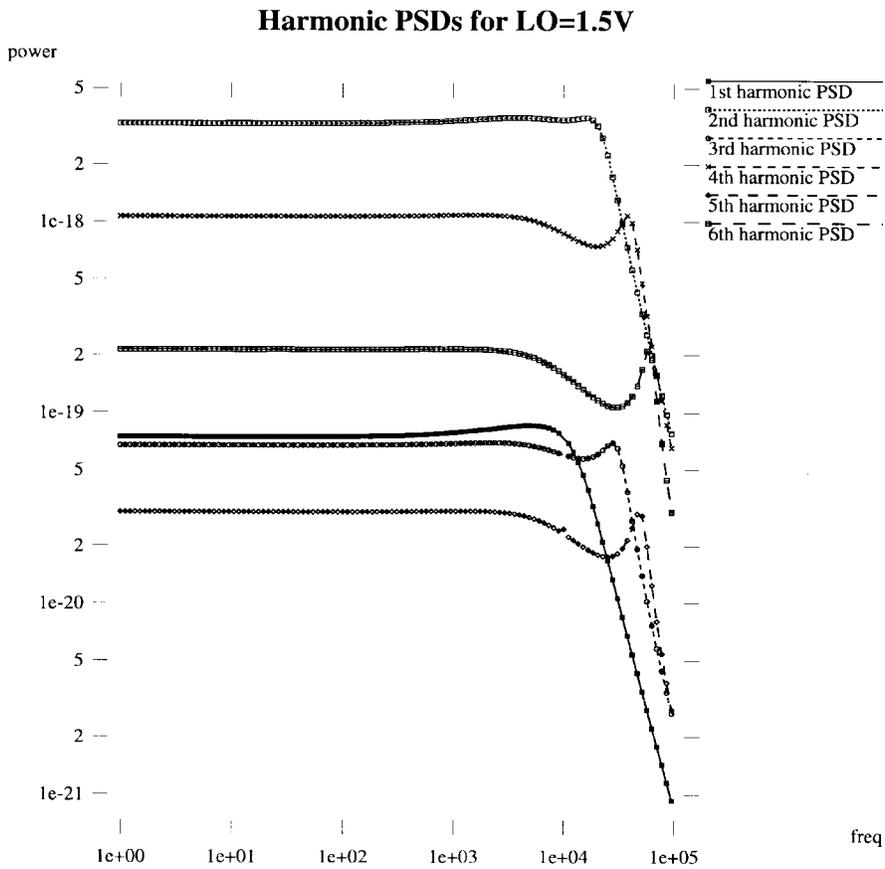
Fig. 15.   Mixer: harmonic PSD's at output.
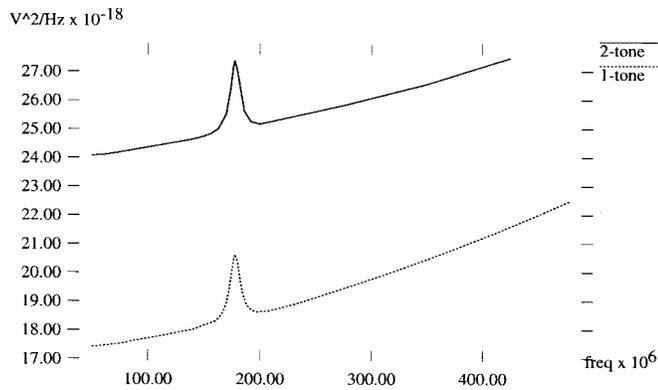
Fig. 16.   Stationary PSD's for the I-Q mixer/buffer circuit.

about 1/3. This is due to *noise folding*, the result of devices being driven into nonlinear regions by the strong RF input tone. This effect is difficult to predict with the technique of, e.g., [4]. The peaks in the two waveforms, located at the LO frequency, are due to up- and down-conversion of noise from other frequencies.

VI. CONCLUSION

A frequency-domain formulation and algorithm has been presented for computing noise in nonlinear circuits. The method uses cyclostationary components and harmonic PSD's in its formulation to capture time-varying noise statistics. A block-structured matrix equation for the output noise statistics is the central result enabling fast computation. The algorithm is efficient for large circuits with several large tones and can generate information useful for noise macromodels.

The new formulation has been used to prove that one-sided bandpass filtering of cyclostationary noise produces stationary noise. This extends a previously known result for low-pass filtering.

The algorithm been verified against Monte Carlo simulations. Results from a mixer cell and a large I-channel buffer and mixer RF integrated circuit have been presented, predicting the fact that the presence of multiple tones can significantly affect the noise performance of a circuit.

REFERENCES

[1] V. Rizzoli, F. Mastri, and D. Masotti, "General noise analysis of nonlinear microwave circuits by the piecewise harmonic-balance technique," *IEEE Trans. Microwave Theory Tech.*, vol. 42, pp. 807–819, May 1994.

[2] A. Demir, E. Liu, and A. Sangiovanni-Vincentelli, "Time-domain non Monte-Carlo noise simulation for nonlinear dynamic circuits with arbitrary excitations," *IEEE Trans. Computer-Aided Design*, vol. 15, pp. 493–505, May 1996.

[3] M. Okumura, H. Tanimoto, T. Itakura, and T. Sugawara, "Numerical noise analysis for nonlinear circuits with a periodic large signal excitation including cyclostationary noise sources," *IEEE Trans. Circuits Syst.–I*, vol. 40, pp. 581–590, Sept. 1993.

[4] R. Telichevesky, K. Kundert, and J. White, "Efficient AC and noise analysis of two-tone RF circuits," in *Proc. IEEE DAC*, 1996, pp. 292–297.

[5] T. Ström and S. Signell, "Analysis of periodically switched linear circuits," *IEEE Trans. Circuits Syst.*, vol. CAS-24, pp. 531–541, Oct. 1977.

[6] A. R. Kerr, "Noise and loss in balanced and subharmonically pumped mixers: Part 1—Theory," *IEEE Trans. Microwave Theory Tech.*, vol. MTT-27, pp. 938–943, Dec. 1979.

[7] W. Gardner, *Introduction to Random Processes*.   New York: McGraw-Hill, 1986.

[8] J. Roychowdhury and P. Feldmann, "A new linear-time harmonic balance algorithm for cyclostationary noise analysis in RF circuits," in *Proc. ASP-DAC*, 1997, pp. 483–492.

[9] A. Papoulis, *Probability, Random Variables and Stochastic Processes*. New York: McGraw-Hill Series in System Science, 1965.

[10] S. A. Haas, *Nonlinear Microwave Circuits*.   Norwood, MA: Artech House, 1988.

[11] R. C. Melville, P. Feldmann, and J. Roychowdhury, "Efficient multitone distortion analysis of analog integrated circuits," in *Proc. IEEE CICC*, May 1995, pp. 241–244.

[12] M. Rösch, "Schnell simulation des stationären Verhaltens nichtlinearer Schaltungen," Ph.D. dissertation, Technischen Universität München, 1992.

[13] H. G. Brachtendorf, G. Welsch, R. Laur, and A. Bunse-Gerstner, "Numerical steady state analysis of electronic circuits driven by multitone signals," *Elect. Eng.*, vol. 79, pp. 103–112, 1996.

[14] R. Freund, G. H. Golub, and N. M. Nachtigal, "Iterative solution of linear systems," *Acta Numerica*, pp. 57–100, 1991.

[15] Y. Saad, *Iterative Methods for Sparse Linear Systems*.   Boston, MA: PWS, 1996.

[16] M. Rösch and K. J. Antreich, "Schnell stationäre simulation nichtlinearer Schaltungen im Frequenzbereich," *AEÜ*, vol. 46, no. 3, pp. 168–172, 1992.

[17] A. Van der Ziel, *Noise in Solid State Devices and Circuits*.   New York: Wiley, 1986.

[18] A. Demir, "Time domain non Monte Carlo noise simulation for nonlinear dynamic circuits with arbitrary excitations," Tech. Rep. Memo. UCB/ERL M94/39, EECS Dept., Univ. Calif. Berkeley, 1994.

[19] V. Rizzoli and A. Neri, "State of the art and present trends in nonlinear microwave CAD techniques," *IEEE Trans. Microwave Theory Tech.*, vol. 32, pp. 343–365, Feb. 1988.

[20] M. Banu, V. Gopinathan, R. Meyer, and Y. Tsividis, Personal communications, 1996.

[21] C. Hull and R. G. Meyer, "A systematic approach to the analysis of noise in mixers," *IEEE Trans. Circuits Syst.–I*, vol. 40, pp. 909–919, Dec. 1993.

[22] J. Roychowdhury and P. Feldmann, "Generating stationary noise for circuit noise simulation," Bell Laboratories Tech. Memo., Oct. 1996.

Jaijeet Roychowdhury received the B.Tech. degree from the Indian Institute of Technology, Kanpur, in 1987 and the M.S. and Ph.D. degrees from the University of California, Berkeley, in 1989 and 1993, all in electrical engineering.

From 1993 to 1995, he was with the CAD Laboratory of AT&T Bell Labs, Allentown, PA. Since 1995, he has been with the Communications Research Division of Bell Laboratories, Murray Hill, NJ. His main research interest is the analysis of dynamical systems, particularly those relevant from circuits and communication systems.

David Long received the B.S. degree from the California Institute of Technology, Pasadena, in 1987 and the Ph.D. degree in computer science from Carnegie Mellon University, Pittsburgh, PA, in 1993.

Since then he has been a Member of the Technical Staff at Bell Laboratories, Murray Hill, NJ. His research interests include circuit simulation, formal verification, and computational electromagnetics.

Peter Feldmann (S'87–M'91–SM'96) was born in Timişoara, Romania. He received the B.Sc. degree *summa cum laude* in computer engineering in 1983 and the M.Sc. degree in electrical engineering in 1987, both from the Technion, Israel, and the Ph.D. degree in 1991 from Carnegie Mellon University, Pittsburgh, PA.

From 1985 through 1987 he worked for Zoran Microelectronics, Haifa, Israel, on the design of digital signal processors. Currently, he is Distinguished Member of Technical Staff at Bell Laboratories, Murray Hill, NJ. His main research interests are simulation and analysis of circuits and communication systems.